Häfner, Stephan; Käske, Martin; Thomä, Reiner:

On calibration and direction finding with uniform circular arrays

Original published in:	International journal of antennas and propagation. - New York, NY : Hindawi. - (2019), art. 1523469, 12 pp.
Original published:	2019-07-03
ISSN:	1687-5877
DOI:	10.1155/2019/1523469
[*Visited:*	2019-08-21]

Hindawi
International Journal of Antennas and Propagation
Volume 2019, Article ID 1523469, 12 pages
https://doi.org/10.1155/2019/1523469

Research Article

On Calibration and Direction Finding with Uniform Circular Arrays

Stephan Häfner, Martin Käske, and Reiner Thomä

Electronic Measurements and Signal Processing Group, Technische Universität Ilmenau, 98684 Ilmenau, Germany

Correspondence should be addressed to Stephan Häfner; stephan.haefner@tu-ilmenau.de

Received 24 February 2019; Revised 15 May 2019; Accepted 27 May 2019; Published 3 July 2019

Academic Editor: Chien-Jen Wang

Antenna array calibration methods and narrowband direction finding (DF) techniques will be outlined and compared for a uniform circular array. DF is stated as an inverse problem, which solution requires a parametric model of the array itself. Because real arrays suffer from mechanical and electrical imperfections, analytic array models are per se not applicable. Mitigation of such disturbances by a global calibration matrix will be addressed, and methods to estimate this calibration matrix will be recapped from literature. Also, a novel method will be presented, which circumvents the problem of a changed noise statistic due to calibration. Furthermore, local calibration, where array calibration measurements are incorporated in the DF algorithm, is considered as well. Common DF algorithms will be outlined, their assumptions regarding array properties will be addressed, and required preprocessing steps such as the beam-space transformation will be presented. Also, two novel DF techniques will be proposed, based on the Capon beamformer, but with reduced computational effort and higher resolution for bearing estimation. Simulations are used to exemplary compare calibration and DF methods in conjunction with each other. Furthermore, measurements with a single and two coherent sources are considered. It turns out that global calibration enables computational efficient DF algorithms but causes biased estimates. Furthermore, resolution of two coherent sources necessitates array calibration.

1. Introduction

Direction finding (DF) is a task which occurs in several applications of surveillance, reconnaissance, radar, or sonar. Basically, DF can be defined as estimation of the bearing of one or multiple signal sources with respect to (w.r.t.) a reference point in space. Typically, an array of spatially distributed sensors is placed at this reference point and the array output is exploited for DF. Hence, DF estimation is an inverse problem. Solving the inverse problem requires a parametric model of the array output in terms of the parameters of interest: azimuth of arrival (AoA) φ and elevation of arrival (EoA) ϑ, which together define the direction of arrival (DoA).

In order to derive a parametric model of the array output, a model of the sensor array itself is necessary. The array model highly depends on the array geometry and the characteristic of each sensor. Theoretical array models typically assume omnidirectional sensors and an ideal array geometry, which cannot be assured for real arrays. Apart from these assumptions, real arrays suffer from disturbances as, e.g., mutual coupling between the sensors or the support structure of the array, unknown sensor gain, and phase or mechanical imperfections [1]. Consequently, DoA estimation performance degrades, because the assumed array model does not coincide with the real array characteristics. Hence, calibration is necessary to mitigate these imperfections.

All investigations are subject to a uniform circular array (UCA). UCAs feature a very attractive geometry, because their aperture covers the whole azimuth range and hence ambiguous free AoA estimates are ensured, on the contrary to, e.g., uniform linear array (ULA). Also, UCAs can be employed to estimate elevation too, but generally not unambiguous. For simplification, only AoA estimation and copolarised sources w.r.t. the array sensors are considered. For the conducted investigations it is not necessary to consider elevation and arbitrarily polarised sources. However, neglecting source polarisation and assuming fix elevation may result in biased estimates in real DF applications [2].

The goal of this paper is to jointly investigate array calibration methods and narrowband DF techniques. Global

calibration, where a direction independent calibration matrix is used, will be considered. Methods to estimate the global calibration matrix from array calibration measurements are reviewed and a new method is proposed, which accounts for the change of the noise statistic due to the application of the calibration matrix. Also, local calibration, where the array calibration data are incorporated in the DF method, is considered. Known DF techniques will be outlined and two novel DF techniques based on the Capon beamformer will be proposed, featuring a reduced computational effort and better resolution in case of multiple sources. Some of the considered DF techniques take advantage of special array structures, which are not provided by UCAs. Hence, beamspace transformation will be briefly recapped. Simulations and measurements are employed for the investigations. Measurements with two coherent sources, hence sources with a fix phase relation, will be considered. Resolution of coherent sources is crucial in DF [3], because of the rank-degeneration of the spatial covariance matrix. Hence, the coherent source case will be used as benchmark to justify calibration necessity and to investigate the DF accuracy.

The reminder of the paper is organised as follows: a parametric model of the array output is derived in Section 2. In Section 3 the DF techniques are presented. The beamspace transformation for UCA is described in Section 4. The problem of array calibration and its influence on the sensor characteristic is presented in Section 5. Simulation based comparison of calibration and DF methods is presented in Section 6. In Section 7, the DF methods are compared using measurements with a single source and two coherent sources. Section 8 concludes the paper.

Mathematical notation is as follows: scalars are italic letters. Vectors are in column format and written as boldface, lower-case, italic letters. Matrices correspond to boldface, upper-case letters. The matrix operations $(.)^T$, $(.)^H$, $(.)^{-1}$, and $(.)^\dagger$ are defined as the transpose, conjugate transpose, inverse, and Moore-Penrose pseudo inverse of a matrix, respectively. The Frobenius norm of a matrix is stated as $\|.\|_F$. The imaginary unit is defined as $\jmath = \sqrt{-1}$.

2. Measurement Data Model

DoA estimation requires a parametric model of the measurement data in terms of the DoAs. Consider an array of M sensors, having its reference point in the origin of a spherical coordinate system. Directions of impinging waves are defined w.r.t. this origin in terms of AoA φ and EoA ϑ; see Figure 1. Consider P plane waves, emerging from far field sources and impinging at the array. The waves are assumed to impinge in the azimuth plane, hence $\vartheta = 0^\circ$ holds. Under narrowband assumption [1, 4], the array output $\mathbf{y}(t) \in \mathbb{C}^{M\times 1}$ in the complex baseband can be approximated as

$$\mathbf{y}(t) \approx \sum_{p=1}^{P} \mathbf{b}\left(\varphi_p\right) \cdot s_p(t) = \mathbf{B}(\boldsymbol{\varphi}) \cdot \mathbf{s}(t), \tag{1}$$

with vector $\mathbf{b}(\varphi_p)$ denoting the narrowband array response w.r.t. the impingement angle φ_p. The narrowband array response is commonly denoted as steering vector. The vectors $\mathbf{s}(t) = [s_1(t), \ldots, s_P(t)]^T \in \mathbb{C}^{P\times 1}$, $\boldsymbol{\varphi} = [\varphi_1, \ldots, \varphi_P]^T \in \mathbb{R}^{P\times 1}$, and matrix $\mathbf{B}(\boldsymbol{\varphi}) = [\mathbf{b}(\varphi_1), \ldots, \mathbf{b}(\varphi_P)] \in \mathbb{C}^{M\times P}$ contain the complex envelope of the source signals, the AoAs of all sources, and the steering vectors, respectively. Measurement noise and uncertainties due to, e.g., model errors are accounted for by an additive error term $\mathbf{n}(t)$. This error term is modelled as a zero-mean and proper complex normal distributed random process, which is spatially white and homogeneous, and uncorrelated with the source signal: $\mathbf{n}(t) \sim \mathcal{CN}(\mathbf{0}, \sigma^2\mathbf{I}_M)$. In summary, the model for the observations $\mathbf{y}(t) \in \mathbb{C}^{M\times 1}$ is [1]

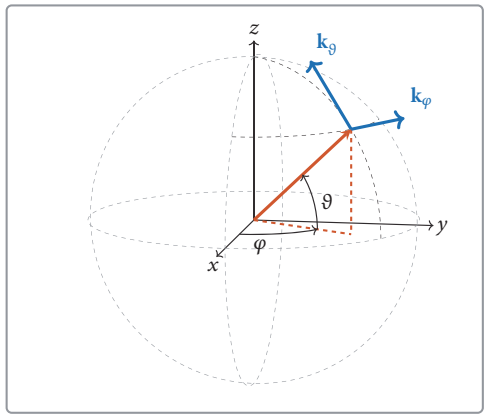

Figure 1: Spherical coordinate system and angle definition.

$$\mathbf{y}(t) = \mathbf{B}(\boldsymbol{\varphi}) \cdot \mathbf{s}(t) + \mathbf{n}(t). \tag{2}$$

In practice N snapshots are taken from the M sensors. Accordingly, the model of the array output becomes

$$\mathbf{Y} = \mathbf{B}(\boldsymbol{\varphi}) \cdot \mathbf{S} + \mathbf{N}. \tag{3}$$

The objective of direction finding is to estimate the AoAs from the array observations $\mathbf{Y} \in \mathbb{C}^{M\times N}$, hence solving the inverse problem. The source directions can be uniquely and ambiguous-freely determined, if this inverse problem is well posed, e.g., the steering matrix features full column rank. In the following, the number of sources P is assumed as known, see, e.g., [5] for a summary of estimation methods.

2.1. UCA Element-Space Model. Consider an uniform circular array with equiangular spaced omnidirectional sensors, placed on a circumference of radius R. The array steering vector entry of the m-th sensor and azimuth only is [6]

$$b_m(\varphi) = \exp\left(\jmath kR\cos\left(\varphi - m\cdot\phi\right)\right), \tag{4}$$

with wave number $k = 2\pi/\lambda_c$, $m = 0, \ldots, M-1$, and the angular spacing of the sensors $\phi = 2\pi/M$. In the following, (4) is referred to as the UCA model in element-space. Practical UCAs do not follow this model due to, e.g., mechanical and electrical imperfections. Hence, calibration is necessary (see Section 5).

Table 1: Considered narrowband DF techniques, the number of identifiable sources, and the considered structure of the steering vectors.

DF Methods	Reference	No. sources	Steering vector
CML	[7, 8]	$\leq M-1$	arbitrary
UML	[7, 8]	$\leq M-1$	arbitrary
MUSIC-1	[9]	$\leq M-1$	arbitrary
root-MUSIC	[10]	$\leq M-1$	Vandermonde
MUSIC-2	[11]	$\leq M-1$	arbitrary
ESPRIT	[12]	$\leq M-1$	Vandermonde
MODE	[8, 13]	$\leq M-1$	arbitrary
IQML	[14]	$\leq M-1$	Vandermonde
Capon-1	[15]	1	arbitrary
Bartlett	[15]	1	arbitrary
root-Capon	This work	1	Vandermonde
Capon-2	This work	1	arbitrary

3. Narrowband Direction Finding Techniques

Several DF techniques are known from literature; see [1, 15] for an overview of the most famous ones. The considered DF methods, the number of sources they are able to resolve, and their assumptions regarding the steering vector structure are summarised in Table 1. The Bartlett and Capon methods are considered to resolve a single source only, because their resolution depends on the array aperture [15]. Hence, the sources have to be well separated in order to resolve them. According to this restriction, the beamformers are not high-resolution estimators and hence not generally applicable for the resolution of multiple sources. However, the beamformers will be used to resolve multiple sources to show the improved estimation capability by calibration. The DF methods constrained maximum-likelihood (CML), unconstrained maximum-likelihood (UML), and Method of Direction Estimation (MODE) require the optimisation of a multidimensional, nonconvex cost function [15]. Optimisation of nonconvex cost functions requires iterative or heuristic methods, which are computational cumbersome and may end up in local optima. The Multiple Signal Classification (MUSIC)-1, Bartlett, and Capon-1 are spectral methods, which require a 1D peak search for DF. The peak search is complicated, if multiple peaks have to be detected to resolve multiple sources. The iterative quadratic maximum-likelihood (IQML), root-MUSIC, MUSIC-2, root-Capon, Capon-2, and Estimation of Signal Parameters via Rotational Invariance Technique (ESPRIT) require polynomial rooting or Eigenvalue decomposition, such that these methods are computationally more efficient. However, some DF methods require a special steering vector structure, which is not fulfilled by an UCA and therefore beam-space transformation is necessary; see Section 4.

3.1. Novel Capon Beamformer Estimators. Generally, the Capon beamformer attempts to minimise the power contribution from interferer directions, while maintaining the gain in the direction of interest. The estimator is given by maximising a 1D spatial spectrum [15]

$$\arg\max_{\varphi} \left[\mathbf{b}(\varphi)^H \cdot \widehat{\mathbf{R}}_{\mathrm{YY}}^{-1} \cdot \mathbf{b}(\varphi)\right]^{-1}. \tag{5}$$

Subsequently, two estimators are proposed, which employ polynomial rooting instead of a 1D peak search to estimate the AoAs from the Capon spectrum. The rooting is computational more efficient, especially if multiple sources shall be resolved and also has a better resolution compared to spectral methods [10].

3.1.1. Root-Capon. Restating cost function (5) as a minimisation problem gives

$$\arg\min_{\varphi} \mathbf{b}(\varphi)^H \cdot \widehat{\mathbf{R}}_{\mathrm{YY}}^{-1} \cdot \mathbf{b}(\varphi). \tag{6}$$

If the steering vectors $\mathbf{b}(\varphi)$ feature Vandermonde structure, minimisation is accomplished by estimating the P roots closest to the unit circle.

3.1.2. Capon-2. Another DF estimator based on the Capon beamformer is derived by exploiting array manifold separation [11]. In manifold separation the array steering vector is decomposed in the product of a vector $\mathbf{d}(\varphi) \in \mathbb{C}^{2L+1\times 1}$ and an array specific sampling matrix $\mathbf{G}$

$$\mathbf{b}(\varphi) = \mathbf{G} \cdot \mathbf{d}(\varphi). \tag{7}$$

Vector $\mathbf{d}(\varphi) = \left[\exp(-\jmath L\varphi), \ldots, \exp(\jmath L\varphi)\right]^T$ features Vandermonde structure and depends on the direction only.

Considering the cost function (6) and plugging in the manifold separation (7) gives

$$\arg\min_{\varphi} \mathbf{d}(\varphi)^H \cdot \mathbf{G}^H \cdot \widehat{\mathbf{R}}_{\mathrm{YY}}^{-1} \cdot \mathbf{G} \cdot \mathbf{d}(\varphi). \tag{8}$$

Again, minimisation is accomplished by estimating the P roots closest to the unit circle.

4. Beam-Space Transformation

The ESPRIT, IQML, root-Capon, and root-MUSIC algorithm are naturally applicable for DF with ULAs. Hence, they necessitate steering vectors with Vandermonde structure. According to (4), the steering vectors of an UCA do not

feature a Vandermonde structure in element-space. Utilising the concept of phase mode excitation [21, 22], the element-space steering vectors are transformed to the beam-space, where the steering vectors feature Vandermonde structure. Phase mode excitation exploits the Jacobi-Anger expansion, which is for the steering vector entry of the m-th sensor

$$\begin{aligned}&\exp\left(\jmath kR\cos\left(\varphi - m\phi\right)\right)\\ &\quad= \sum_{n=-\infty}^{\infty} \jmath^n \cdot J_n\left(kR\right)\cdot\exp\left(\jmath n\varphi\right)\cdot\exp\left(-\jmath m\phi\right),\end{aligned} \tag{9}$$

with J_n being the Bessel function of first kind and n-th order. Approximating the infinite series by a finite one yields

$$\begin{aligned}&\exp\left(\jmath kR\cos\left(\varphi - m\phi\right)\right)\\ &\quad\approx \sum_{n=-M'}^{M'} \jmath^n \cdot J_n\left(kR\right)\cdot\exp\left(\jmath n\varphi\right)\cdot\exp\left(-\jmath nm\phi\right)\\ &\quad= \mathbf{d}\left(m\phi\right)^T\cdot\mathbf{V}\cdot\mathbf{a}\left(\varphi\right),\end{aligned} \tag{10}$$

with $M' = \lfloor (M-1)/2 \rfloor$ [3] and

$$\mathbf{d}\left(m\phi\right) = \left[\exp\left(-\jmath M' m\phi\right),\ldots,\exp\left(\jmath M' m\phi\right)\right]^T \tag{11a}$$

$$\mathbf{V} = \operatorname{diag}\left\{\left[\jmath^{-M'} J_{-M'}\left(kR\right),\ldots,\jmath^{M'} J_{M'}\left(kR\right)\right]\right\} \tag{11b}$$

$$\mathbf{a}\left(\varphi\right) = \left[\exp\left(-\jmath M'\varphi\right),\ldots,\exp\left(\jmath M'\varphi\right)\right]^T. \tag{11c}$$

Vector $\mathbf{a}(\varphi)$ denotes the Vandermonde structured steering vector in beam-space. The truncated Jacobi-Anger expansion for the array steering vector according to (4) is

$$\mathbf{b}\left(\varphi\right) = \mathbf{D}^T\cdot\mathbf{V}\cdot\mathbf{a}\left(\varphi\right), \tag{12}$$

with matrix $\mathbf{D} = \left[\mathbf{d}(0\phi),\ldots,\mathbf{d}((M-1)\phi)\right] \in \mathbb{C}^{2M'+1\times M}$ being the Discrete Fourier Transform (DFT) matrix. The phase mode excitation or beam-space transformation is now given by

$$\left(\mathbf{D}^T\cdot\mathbf{V}\right)^{\dagger}\cdot\mathbf{b}\left(\varphi\right) = \mathbf{a}\left(\varphi\right). \tag{13}$$

In order to yield the array output in beam-space $\mathbf{y}_{\mathrm{BS}}(t)$, the transformation is applied to the array output $\mathbf{y}(t)$

$$\mathbf{y}_{\mathrm{BS}}\left(t\right) = \left(\mathbf{D}^T\cdot\mathbf{V}\right)^{\dagger}\cdot\mathbf{y}\left(t\right). \tag{14}$$

The truncated Jacobi-Anger expansion introduces a systematic error, which depends on the actual AoA and causes an estimation bias or increased estimation variance [23]. Furthermore, beam-space transformation changes the second-order statistic of the noise, which is no longer homogeneous over the array channels.

The beam-space transformation assumes an UCA, which follows the element-space model (4). This model does not apply for real arrays, such that calibration of the array is necessary.

5. Sensor Array Calibration

5.1. Global vs. Local Array Calibration

5.1.1. Global Calibration. In global calibration, the disturbed array output is mapped onto a reference array output, whereas the disturbances are assumed as independent on the direction of impingement. In the following, a linear relationship between disturbed and reference array output is assumed. Then, global array calibration is done by a calibration matrix $\mathbf{C} \in \mathbb{C}^{M\times M}$, mapping the reference array output $\mathbf{m}(\varphi)$ onto the disturbed one $\widetilde{\mathbf{m}}(\varphi)$

$$\mathbf{C}^{-1} : \mathbf{m}\left(\varphi\right) \longmapsto \widetilde{\mathbf{m}}\left(\varphi\right). \tag{15}$$

Accordingly, calibration of the array is given by

$$\mathbf{y}_c\left(t\right) = \mathbf{C}\cdot\mathbf{y}\left(t\right), \tag{16}$$

with the vector $\mathbf{y}_c(t)$ of calibrated array outputs. Note that applying the calibration matrix changes the second-order statistics of the noise, which becomes $\sigma^2\mathbf{C}\mathbf{C}^H$. In the simulation and measurement section it will not be accounted for the changed noise statistics, in order to investigate the influence of global calibration on the estimator performance.

The calibration matrix is derived from array calibration measurements, which are conducted on a test range or in an anechoic chamber. These measurements are a set of array outputs for known directions of impingement and comprise the array characteristics as well as the disturbances. Introduce the matrices

$$\mathbf{B}^{\mathrm{ref}}\left(\boldsymbol{\varphi}\right) = \left[\mathbf{b}^{\mathrm{ref}}\left(\varphi_1\right),\ldots,\mathbf{b}^{\mathrm{ref}}\left(\varphi_V\right)\right] \in \mathbb{C}^{M\times V} \tag{17a}$$

$$\mathbf{B}\left(\boldsymbol{\varphi}\right) = \left[\mathbf{b}\left(\varphi_1\right),\ldots,\mathbf{b}\left(\varphi_V\right)\right] \in \mathbb{C}^{M\times V} \tag{17b}$$

$$\mathbf{A}\left(\boldsymbol{\varphi}\right) = \left[\mathbf{a}\left(\varphi_1\right),\ldots,\mathbf{a}\left(\varphi_V\right)\right] \in \mathbb{C}^{M\times V}, \tag{17c}$$

whereas $\mathbf{B}^{\mathrm{ref}}$ comprises the steering vectors from the calibration measurements, and $\mathbf{B}$ and $\mathbf{A}$ comprise the steering vectors from the sampled element- and beam-space array model, respectively. The calibration matrix can be calculated in element- and beam-space. Considering the array model in element-space, the calibration matrix is calculated in element-space.

$$\mathbf{C}_{\mathrm{ES}} : \mathbf{B}^{\mathrm{ref}}\left(\boldsymbol{\varphi}\right) \longmapsto \mathbf{B}\left(\boldsymbol{\varphi}\right) \tag{18}$$

Application of matrix $\mathbf{C}_{\mathrm{ES}}$ to the array output yields the calibrated array output in element-space. Hence, subsequent transformation to beam-space may be necessary depending on the AoA estimator. Considering the array model in beam-space, the calibration matrix is calculated in beam-space.

$$\mathbf{C}_{\mathrm{BS}} : \mathbf{B}^{\mathrm{ref}}\left(\boldsymbol{\varphi}\right) \longmapsto \mathbf{A}\left(\boldsymbol{\varphi}\right) \tag{19}$$

Application of matrix $\mathbf{C}_{\mathrm{BS}}$ to the array output yields the calibrated array output in beam-space.

Table 2: Considered methods to estimate calibration matrix **C**.

Method	Reference	Estimation space
Wax	[3]	element- and beam-space
Sommerkorn	[16]	element- and beam-space
Kortke	[17]	element- and beam-space
Friedlander	[18]	element-space
Ng	[19]	element-space
See	[20]	element- and beam-space
Haefner	This work	element- and beam-space

5.1.2. Local Calibration. In local calibration, the array disturbances are considered as depending on the direction of impingement. Consideration of direction dependent disturbances is accomplished by using the array calibration measurements $\mathbf{B}^{\text{ref}}(\boldsymbol{\varphi})$ as the reference steering vectors in the DF algorithms [2, 24]. Consequently, the estimators ESPRIT, IQML, root-MUSIC, and root-Capon are not applicable under local calibration, because these methods cannot incorporate arbitrary or measured steering vectors [15].

Because the calibration measurements describe the array for discrete angles only, whereas DF algorithms require a continuous description, interpolation is required. Here, the EADF [25] is used to interpolate the calibration measurements.

5.2. Estimation of Global Calibration Matrix. Table 2 summarises the considered methods to estimate the global calibration matrix. Depending on the considered array model and the estimation method, the calibration matrix can be estimated in element- or beam-space.

5.2.1. Haefner-Method. As pointed out, the second-order statistic of the noise is changed by applying the calibration matrix. This can deteriorate the performance of some DF methods, because they assume the noise covariance matrix to be diagonal. Introducing the constrain $\mathbf{C}\mathbf{C}^H = \mathbf{I}$ regarding the estimation of the calibration matrix, the noise statistic will not change after calibration. Applying this constraint to the method of Wax results in novel method to estimate the calibration matrix.

$$\begin{aligned} \arg\min_{\mathbf{C}} \quad & \left\| \mathbf{C} \cdot \mathbf{B}^{\text{ref}}(\boldsymbol{\varphi}) - \mathbf{M}(\boldsymbol{\varphi}) \right\|_{\text{F}}^2, \\ \text{s.t.} \quad & \mathbf{C}\mathbf{C}^H = \mathbf{I} \end{aligned} \tag{20}$$

Hence, the objective is to minimise the cost function subject to the constraint that the resulting matrix is unitary [26].

5.3. Impact of Global Calibration on Array Characteristics. In order to investigate the effect of calibration on the array characteristic, a real array will be considered. The array under consideration is the Poynting DF-A0046 UCA (see Figure 2), which operates at 305 MHz centre frequency. The array features 5 vertically polarised dipoles and 5 horizontally polarised monopoles, whereas the dipoles will be considered only.

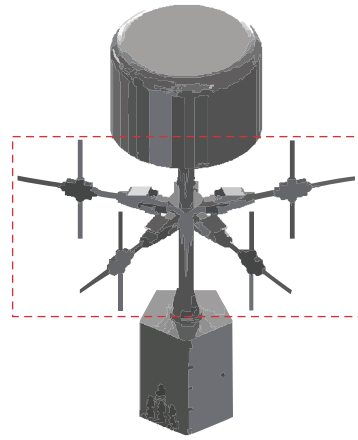

Figure 2: Poynting DF-A0046 UCA (dashed box) featuring 5 vertically polarised dipoles and 5 horizontally polarised monopoles. Only the dipoles will be considered in this paper.

First, the influence of global calibration on the array geometry is investigated. As stated previously, practical arrays suffer from mechanical imperfections, such that the assumed circular geometry is not assured. The estimated and assumed sensor positions are shown in Figure 3. It becomes obvious that the real array does not feature UCA properties as, e.g., equiangular spaced sensors. After calibration the sensor positions are slightly corrected. Hence, geometrical imperfections can be corrected to some extent by global calibration.

Furthermore, the effect of calibration on the sensor characteristics is investigated. Magnitude and phase of the model and the sensor response before and after calibration are shown in Figures 4(a) and 4(b), respectively. From Figure 4(a) it becomes obvious that the vertical dipole is shadowed by the array mast, resulting in an attenuation of up to 10 dB. After calibration, this strong attenuation is corrected, resulting in a more omnidirectional characteristic of the sensor. Also, the direction cosine of the phase becomes much closer to the model after calibration; see Figure 4(b).

6. Simulation Based Studies

In order to compare the various calibration matrix estimators and the DF techniques, Monte-Carlo simulations with varying signal to noise ratio (SNR) are carried out. Data are

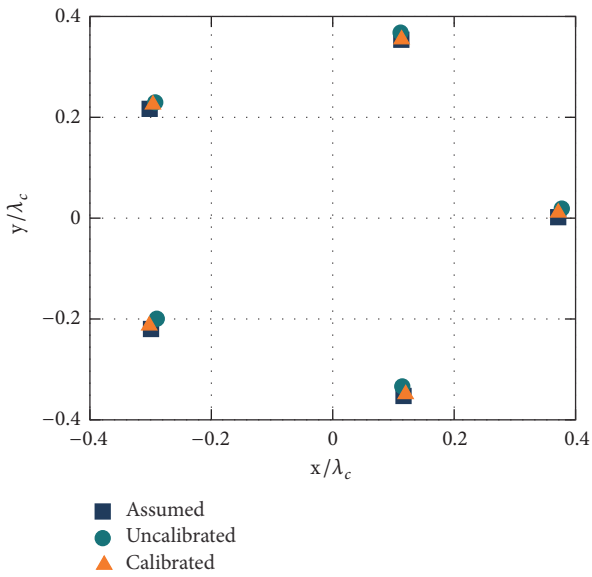

Figure 3: Normalised sensor positions in the x-y-plane (array top view) as assumed by the model, and before and after global calibration. The sensor positions are normalised to the centre wavelength λ_c.

Table 3: Parameters of the simulations.

Parameter	Value
Transmit signal	zero-mean, circularly normal distributed
Centre frequency	305 MHz
Receive array	Poynting DF-A0046
SNR	−10 dB to 40 dB
No. snapshots	50
AoAs	uniformly distributed

generated according to (3), whereas a single source is considered. The simulation parameters are summarised in Table 3. As receive array the Poynting DF-A0046 UCA is used, and calibration data of the array are used as steering vectors for the generation of the data. Figure of merit for comparison is the root mean-square error (RMSE) of AoA estimates. The estimation error is defined as the orthodromic angular distance ζ between the given AoA φ and the estimated AoA $\widehat{\varphi}$

$$\zeta = \arccos\left(\cos\left(\left|\varphi - \widehat{\varphi}\right|\right)\right). \tag{21}$$

The RMSE is calculated by averaging the squared estimation error over 1000 Monte-Carlo runs, whereas each run features fix SNR and random AoA. The derived RMSEs are compared to the stochastic Cramér-Rao lower bound (CRLB) [27], indicating the lowest achievable RMSE for an unbiased estimator.

6.1. Comparison of Calibration Matrix Estimators. The estimated global calibration matrices are applied to the generated array outputs and DF is conducted afterwards. The ESPRIT estimator and the MUSIC-1 estimator are exemplary utilised for AoA estimation in beam-space and element-space, respectively. For the ESPRIT estimator, calibration according to the array model in beam- and element-space with subsequent beam-space transformation is applied. The resulting RMSEs are shown in Figures 5(b) and 5(a). The RMSEs for MUSIC-1 based estimation are shown in Figure 6.

Obviously, the RMSE curves for all calibration methods converge to a certain value, indicating biasedness. Furthermore, the ESPRIT estimates never attain the CRLB, because the beam-space transformation introduces errors resulting in an increased variance of the estimates. Furthermore, the RMSEs of the ESPRIT estimates indicate that calibration w.r.t. the array model in element-space slightly outperforms the calibration w.r.t. the array model in beam-space. An explanation can be given by the global calibration matrix itself. Basically, the matrix describes disturbances due to coupling or electrical and mechanical imperfections. Therefore, the calibration matrix has a clear physical meaning in the element-space. Calibration matrix estimation w.r.t. to the beam-space model assumes a virtual array, such that the calibration matrix has no longer a clear physical meaning. Hence, the disturbances are not described properly and the calibration becomes less powerful. The proposed estimation method performs comparably worse, which can be related to the constraint of a Hermitian calibration matrix causing a less powerful calibration. Hence, variation of the noise statistic is not as a crucial for the bearing estimation as remaining calibration errors. Comparison of the RMSEs of the ESPRIT and MUSIC-1 estimator indicates that the MUSIC-1 estimator attains the CRLB for SNRs around 0 dB, but the ESPRIT estimator slightly outperforms the MUSIC-1 estimator in terms of minimal achievable RMSE. Overall, the estimation method by Sommerkorn in conjunction with the ESPRIT performs best.

6.2. Comparison of DF Techniques. First, the considered DF techniques in conjunction with global calibration will be compared. The global calibration matrix is estimated in element-space by the method of Sommerkorn. The calculated RMSEs are shown in Figure 7(a). All estimators saturate to a certain RMSE for high SNRs, such that the estimators in conjunction with the global calibration are not considerable as unbiased. Because of, e.g., the erroneous sensor positions due to mechanical imperfections, array disturbances are direction dependent. However, global calibration attempts to correct the array disturbances according to an average disturbance over the whole range of impingement directions. Hence, some model errors remain after calibration, such that the estimators cannot be unbiased. The CML, UML, MODE, MUSIC-1, MUSIC-2, and Bartlett beamformer attain the CRLB for SNRs from −5 dB to 5 dB. Hence, remaining model errors are hidden by the noise in that region, such that model errors are only severe for high SNRs. Overall, the ESPRIT estimator shows the best performance. Hence, the errors due to beam-space transformation are not so severe as the remaining errors from the global calibration. The proposed root-Capon and Capon-2 and the literature based Capon-1 estimator perform comparably worse. Since all Capon methods employ the inverse of the covariance of

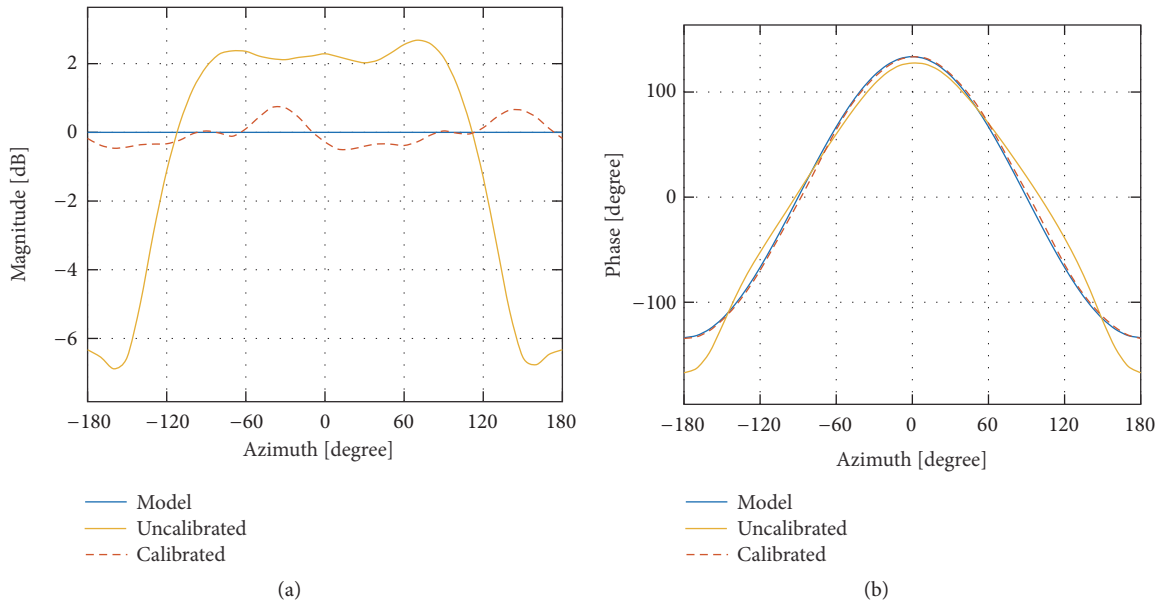

FIGURE 4: Measured response of the first sensor of the Poynting DF-A0046 UCA, the corresponding response of the element-space model and the sensor response after calibration with the calibration matrix estimated by the method of Wax. The plots show the (a) magnitude and (b) phase of the response.

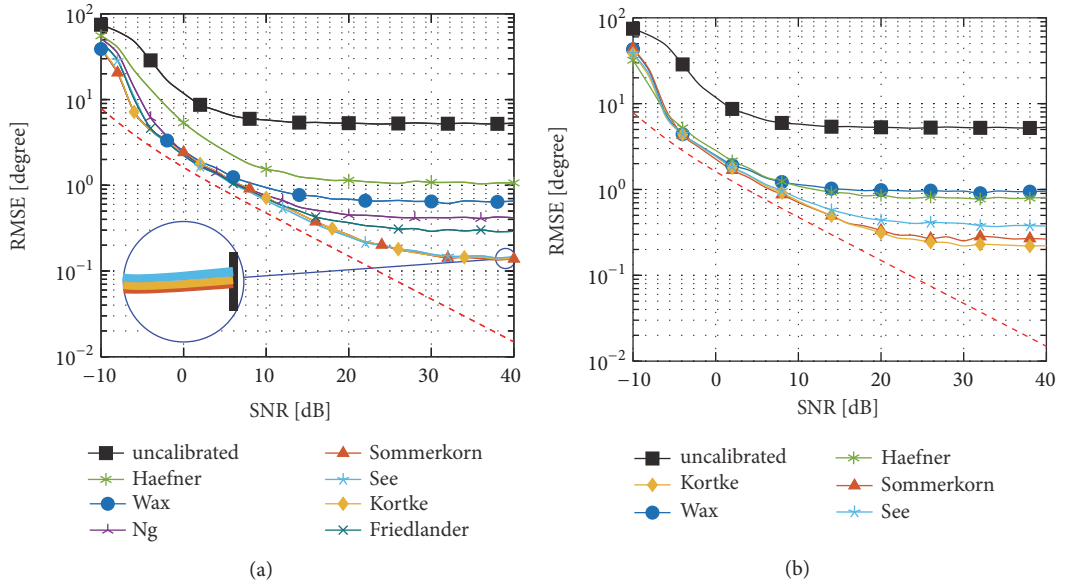

FIGURE 5: RMSE of AoA estimates with the ESPRIT algorithm and calibration w.r.t. (a) the element-space model and subsequent beam-space transformation and (b) the beam-space model. The CRLB is plotted as red dashed line.

the measurements and the calibration matrix influences this covariance, a deteriorated estimation performance seems to be caused by calibration.

In order to verify the explanation of biased estimates due to global calibration, the RMSE for local calibration will be investigated. Note that the beam-space estimators are excluded, because they cannot be applied under local calibration. The calculated RMSEs are depicted in Figure 7(b). The estimators do not saturate to a certain RMSE and hence are considerable as unbiased. Furthermore, the CRLB is attained by all DF methods for SNRs above 0 dB. Hence, the DF methods are considerable as statistically efficient [15]. Comparing Figures 7(b) and 7(a) it can be concluded that a SNR above 10 dB is sufficient to outperform global calibration by local calibration.

7. Measurement Based Studies

Calibration and experimental measurements were performed on a test range in Paardefontein, South Africa, using the

Table 4: Setup for the test measurements.

Parameter	Value
Transmit signal	multi–sine
Centre frequency	305 MHz
Bandwidth	10 MHz
Transmit antennas	logarithmic periodic dipole antenna
Transmit polarisation	vertical
SNR	approx. 25 dB
Receive array	uniform circular array with 5 dipols
Receive polarisation	vertical
AoAs	25°; 25° & −30°; 8° & −10°

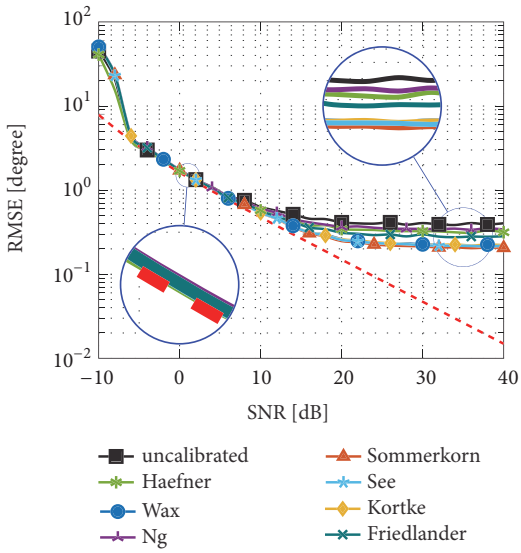

Figure 6: RMSE of AoA estimates with the MUSIC-1 algorithm and calibration w.r.t. the element-space model. The CRLB is plotted as red dashed line.

5 vertically polarised dipoles of the Poynting DF-A0046 UCA as receive array. First, a single source has been placed at 25° azimuth angle and approx. 102 m apart from the receiving array. Afterwards, a second source has been placed at −30° azimuth angle and approx. 72 m apart from the receiving array. The second source is driven by the same signal as the first one, such that the phase difference between both sources remains fixed (coherent source case). To cope with the presence of coherent sources, spatial smoothing in conjunction with forward-backward averaging is applied as a preprocessing step [28] for the ESPRIT and root-MUSIC estimator. Last, two coherent sources were placed at −10° and 8° azimuth angle and 91 m and 61 m apart from the receiver, respectively. The elevation angles in all measurements were approx. 0°. Some details of the measurement setup can be found in [24]. Source antennas were vertically polarised logarithmic periodic dipole antenna (LPDA). Transmit signal was a multi-sine signal with 10 MHz bandwidth at a carrier frequency of 305 MHz. The measurement setup is summarised in Table 4.

To show the difference between global and local calibration, the spectrum of the Bartlett, Capon-1, and MUSIC-1 method is calculated for both calibration schemes. The respective spectra for the measurement with the single source are shown in Figure 8. Obviously, local calibration results in more sharpened peaks in the Capon spectrum and reduced side lobes in the Bartlett spectrum.

First, the estimators are applied to the measurements without previous calibration. The estimation results for the single and dual source measurement are shown in Table 5. The maximum-likelihood estimators (CML, UML, and MODE), the MUSIC type estimators (MUSIC-1; MUSIC-2), and the Bartlett beamformer are able to resolve the single source, whereas the Capon beamformers (Capon-1; Capon-2) and the beam-space estimators (ESPRIT, IQML, root-MUSIC, and root-Capon) show poor results. However, all DF methods fail to properly estimate the AoAs in case of two coherent sources. Hence, estimating the directions of two coherent sources requires array calibration.

The method by Sommerkorn is utilised to estimate the global calibration matrix in element-space. Estimated AoAs for the single and dual source case are shown in Table 6. In the single source case, all estimators show good estimation results for global as well as local calibration. In the dual source case, the maximum-likelihood and MUSIC estimators show the best accuracy for global calibration. The Capon and Bartlett methods fail to resolve the sources. Facing the beam-space estimators, only the ESPRIT shows considerable good results. An explanation is the beam-space transformation and the few number of sensors, which causes biased estimates [23]. In case of local calibration, all applied estimators show good estimation results for the dual source case. Note that the Capon beamformers properly resolve both sources under local calibration, whereas the Bartlett beamformer fails. An explanation is the reduced leakage of the Capon beamformer compared to the Bartlett [15].

Last, the scenario with the closer located sources is considered. The estimation results are shown in Table 7. Obviously, the beam-space estimators fail. Comparing the estimates for global and local calibration indicates an improved accuracy by local calibration. Furthermore, the proposed Capon-2 method is able to slightly resolve both sources, whereas the Bartlett and Capon-1 method fails.

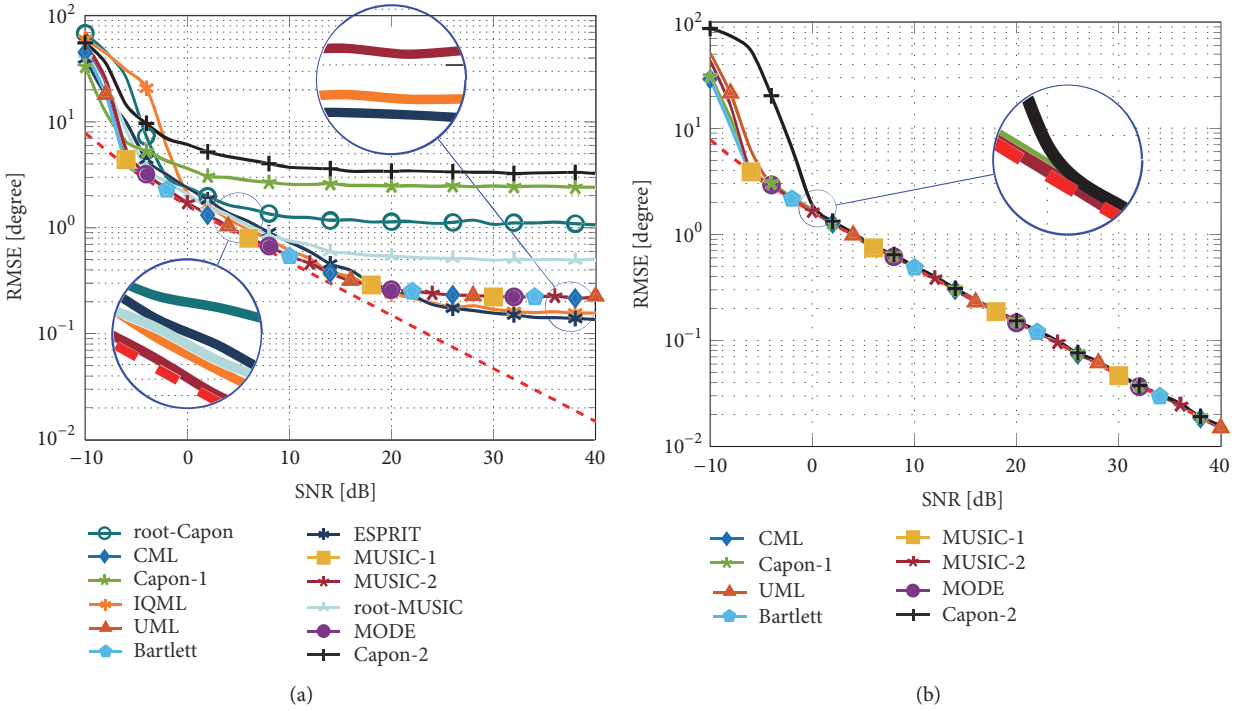

Figure 7: RMSE of AoA estimation with several DF techniques for (a) global calibration using the method of Sommerkorn to estimate the calibration matrix and (b) local calibration using the EADF as array model. The CRLB is plotted as red dashed line.

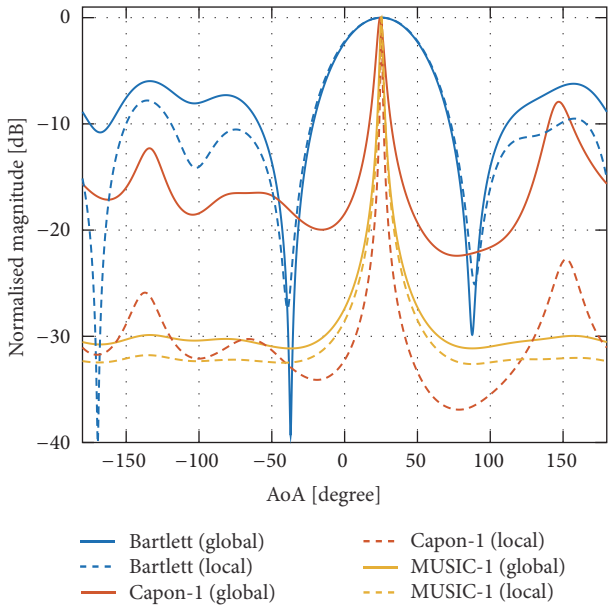

Figure 8: Spectra of Bartlett beamformer, Capon-1 beamformer, and MUSIC-1 for global and local calibration. The global calibration matrix has been calculated by the method of Sommerkorn. Measurement data with a single source at 25° are used to calculate the spectra.

In summary, calibration is not necessary in the single source case, because some estimators can tackle the array disturbances. However, calibration is required in case of two coherent sources. Furthermore, beam-space methods are quite sensitive due to the beam-space transformation and the few number of sensors, such that these methods are not able to resolve two closely spaced sources. Overall, DF methods in conjunction with local calibration show the best estimation accuracy.

8. Conclusion

Calibration of and direction finding with uniform circular arrays has been investigates in this paper. Several assumptions have been drawn for the conducted investigations. First, source signals are assumed to imping in the azimuth plane. Second, cross-polar sensor characteristics have been neglected, because the sources are assumed to be copolar.

Global and local calibration of the UCA have been investigated. As shown by simulations, DF in conjunction with global calibration results in biased estimates due to remaining model errors, which are especially severe for high SNRs. On the contrary, DF in conjunction with local calibration results in unbiased estimates. Also, it was shown that local calibration is superior to global calibration in terms of the achievable root mean-square error for SNR above 10 dB. Furthermore, test measurements with a single and two coherent sources have been considered. In case of a single source, array calibration is not necessary for several estimation methods. However, calibration was found to be required in order to resolve coherent sources. Also, local calibration was found to outperform global calibration in case of closely spaced coherent sources. Comparison of the DF techniques based on simulations and test measurements

Table 5: Estimated AoAs without array calibration. The setup is a single source (25°) and a coherent dual source (−30°, 25°) scenario.

Estimator	*Single Source*	*Dual Source*	
	AoA [°]	*AoA* [°]	*AoA* [°]
ESPRIT	29.82	−61.17	52.91
root-MUSIC	22.22	−50.01	44.05
IQML	26.38	−24.03	79.29
root-Capon	29.41	−39.36	38.82
Capon-1	28.42	−39.99	35.64
Bartlett	25.04	−135.28	16.06
MUSIC-1	25.04	−33.98	28.82
CML	25.04	−33.25	22.4
UML	25.04	−178.18	102.63
MODE	25.04	−34.24	22.08
Capon-2	28.42	−40.69	35.82
MUSIC-2	25	−35.12	29.8

Table 6: Estimated AoAs under global and local array calibration. The setup is a single source (25°) and a coherent dual source (−30°, 25°) scenario.

Estimator	*Calibration*	*Single Source*	*Dual Source*	
		AoA [°]	*AoA* [°]	*AoA* [°]
ESPRIT	global	25.17	−31.18	25.39
root-MUSIC	global	25.66	−27.5	23.26
IQML	global	25.19	−27.7	26.04
root-Capon	global	25.82	−26.3	24.42
Capon-1	global	24.4	−23.81	20.17
Bartlett	global	25.15	−138.18	15.93
MUSIC-1	global	25.15	−30.42	25.46
CML	global	25.15	−30.2	25.8
UML	global	25.15	−30.2	25.8
MODE	global	25.15	−30.2	25.8
Capon-2	global	24.39	−23.55	20.09
MUSIC-2	global	25.14	−30.45	25.48
Capon-1	local	25.31	−30.1	25.13
Bartlett	local	25.37	−134.48	15.4
MUSIC-1	local	25.37	−30.09	25.56
CML	local	25.37	−30.17	25.89
UML	local	25.37	−30.17	25.89
MODE	local	25.37	−30.17	25.89
Capon-2	local	25.31	−30.12	25.18
MUSIC-2	local	25.37	−30.11	25.59

indicates that maximum-likelihood estimators (CML, UML, and MODE) and MUSIC type estimators (MUSIC-1 and MUSIC-2) show better estimation accuracies than beam-space estimators (ESPRIT, IQML, and root-MUSIC).

In summary, choosing the appropriate DF technique and calibration method is an application specific trade-off between required estimation accuracy, computational complexity, and also calibration measurement effort.

Data Availability

The used data have not been made available due to confidentiality agreements with research collaborators.

Conflicts of Interest

The authors declare that they have no conflicts of interest.

Table 7: Estimated AoAs under global and local array calibration. The setup is a coherent dual source (−10°, 8°) scenario.

Estimator	*Calibration*	*Dual Source*	
		AoA [°]	*AoA* [°]
ESPRIT	global	−22.27	19.86
root-MUSIC	global	−17.78	13.62
IQML	global	−22.73	19.72
root-Capon	global	−161.45	−7.61
Capon-1	global	−16.88	15.62
Bartlett	global	2.5	177.67
MUSIC-1	global	−10.69	9.78
CML	global	−10.69	9.72
UML	global	−10.69	9.72
MODE	global	−10.69	9.72
Capon-2	global	−16.91	15.66
MUSIC-2	global	−11.23	10.18
Capon-1	local	−10.03	6.87
Bartlett	local	2.61	177.86
MUSIC-1	local	−9.79	8.44
CML	local	−9.81	8.83
UML	local	−9.81	8.83
MODE	local	−9.81	8.83
Capon-2	local	−10.61	9.7
MUSIC-2	local	−10.34	9.46

Acknowledgments

This work was partially funded by the Bundesministerium für Bildung und Forschung [grant number 16BN1203]. Stephan Häfner is funded by the Deutsche Forschungsgemeinschaft [grant number 317632307]. The authors acknowledge support for the Article Processing Charge by the German Research Foundation (DFG) and the Open Access Publication Fund of the Technische Universität Ilmenau. The authors like to thank Dipl.-Ing Uwe Trautwein for supporting the calibration and test measurements.

References

[1] T. E. Tuncer and B. Friedlander, *Classical and Modern Direction-of-Arrival Estimation*, Academic Press, Amsterdam, Netherlands, 2009.

[2] M. Landmann, M. Kaske, and R. S. Thoma, "Impact of incomplete and inaccurate data models on high resolution parameter estimation in multidimensional channel sounding," *IEEE Transactions on Antennas and Propagation*, vol. 60, no. 2, pp. 557–573, 2012.

[3] M. Wax and J. Sheinvald, "Direction finding of coherent signals via spatial smoothing for uniform circular arrays," *IEEE Transactions on Antennas and Propagation*, vol. 42, no. 5, pp. 613–620.

[4] S. Häfner and R. Thomä, "Application of tensor decomposition methods to antenna array calibration measurements for denoising and narrowband modelling," in *Proceedings of the 13th European Conference on Antennas and Propagation (EuCAP)*, pp. 1–5, 2019.

[5] J. da Costa, A. Thakre, F. Roemer, and M. Haardt, "Comparison of model order selection techniques for high-resolution parameter estimation algorithms," in *Proceedings of the 54th Internationales Wissenschaftliches Kolloquium*, September 2009.

[6] C. A. Balanis, *Antenna Theory: Analysis and Design*, John Wiley Sons, 2nd edition, 1997.

[7] P. Stoica and A. Nehorai, "Performance study of conditional and unconditional direction-of-arrival estimation," *IEEE Transactions on Acoustics, Speech, and Signal Processing*, vol. 38, no. 10, pp. 1783–1795, 1990.

[8] P. Stoica and K. C. Sharman, "Maximum likelihood methods for direction-of-arrival estimation," *IEEE Transactions on Signal Processing*, vol. 38, no. 7, pp. 1132–1143, 1990.

[9] R. Schmidt, "Multiple emitter location and signal parameter estimation," *IEEE Transactions on Antennas and Propagation*, vol. 34, no. 3, pp. 276–280, 1986.

[10] B. D. Rao and K. V. S. Hari, "Performance analysis of root-music," *IEEE Transactions on Signal Processing*, vol. 37, no. 12, pp. 1939–1949, 1989.

[11] F. Belloni, A. Richter, and V. Koivunen, "DoA estimation via manifold separation for arbitrary array structures," *IEEE Transactions on Signal Processing*, vol. 55, no. 10, pp. 4800–4810, 2007.

[12] R. Roy and T. Kailath, "ESPRIT-estimation of signal parameters via rotational invariance techniques," *IEEE Transactions on Signal Processing*, vol. 37, no. 7, pp. 984–995, 1989.

[13] P. Stoica and K. Sharman, "Novel eigenanalysis method for direction estimation," *IEEE Proceedings - Radar and Signal Processing*, vol. 137, no. 1, pp. 19–26, 1990.

[14] Y. Bresler and A. Macovski, "Exact maximum likelihood parameter estimation of superimposed exponential signals in noise," *IEEE Transactions on Signal Processing*, vol. 34, no. 5, pp. 1081–1089, 1986.

[15] H. Krim and M. Viberg, "Two decades of array signal processing research: the parametric approach," *IEEE Signal Processing Magazine*, vol. 13, no. 4, pp. 67–94, 1996.

[16] G. Sommerkorn, D. Hampicke, R. Klukas et al., "Uniform rectangular antenna array design and calibration issues for 2-D ESPRIT application," in *Proceedings of the in 4th European Personal and Mobile Communications Conference, EPMCC*, vol. 1, pp. 169–173, February 2001.

[17] A. Kortke, "A new calibration algorithm for smart antenna arrays," in *Proceedings of the 57th IEEE Semiannual Vehicular Technology Conference. VTC 2003*, vol. 2, pp. 1030–1034, Jeju, South Korea, 2003.

[18] B. Friedlander and A. Weiss, "Direction finding in the presence of mutual coupling," *IEEE Transactions on Antennas and Propagation*, vol. 39, no. 3, pp. 273–284.

[19] B. C. Ng and C. M. Samson, "Sensor-array calibration using a maximum-likelihood approach," *IEEE Transactions on Antennas and Propagation*, vol. 44, no. 6, pp. 827–835, 1996.

[20] C. M. S. See, "Sensor array calibration in the presence of mutual coupling and unknown sensor gains and phases," *IEEE Electronics Letters*, vol. 30, no. 5, pp. 373-374, 1994.

[21] A. Tewfik and W. Hong, "On the application of uniform linear array bearing estimation techniques to uniform circular arrays," *IEEE Transactions on Signal Processing*, vol. 40, no. 4, pp. 1008–1011, 1992.

[22] C. Mathews and M. Zoltowski, "Direction finding with circular arrays via phase mode excitation and Root-MUSIC," in *Proceedings of the IEEE Antennas and Propagation Society International*

Symposium 1992 Digest, vol. 2, pp. 1019–1022, Chicago, IL, USA, June 1992.

[23] F. Belloni and V. Koivunen, "Beamspace transform for UCA: error analysis and bias reduction," *IEEE Transactions on Signal Processing*, vol. 54, no. 8, pp. 3078–3089, 2006.

[24] S. Häfner, M. Käske, R. S. Thomä et al., "Selection of antenna array configuration for polarimetric direction finding in correlated signal environments," in *Proceedings of the 19th International ITG Workshop on Smart Antennas*, pp. 1–8, March 2015.

[25] M. Landmann and G. Del Galdo, "Efficient antenna description for MIMO channel modelling and estimation," in *Proceedings of the 7th European Conference on Wireless Technology, ECWT2004*, pp. 217–220, October 2004.

[26] T. Abrudan, J. Eriksson, and V. Koivunen, "Conjugate gradient algorithm for optimization under unitary matrix constraint," *Signal Processing*, vol. 89, no. 9, pp. 1704–1714, 2009.

[27] P. Stoica, E. G. Larsson, and A. B. Gershman, "The stochastic CRB for array processing: a textbook derivation," *IEEE Signal Processing Letters*, vol. 8, no. 5, pp. 148–150, 2001.

[28] R. T. Williams, S. Prasad, A. K. Mahalanabis, and L. H. Sibul, "An improved spatial smoothing technique for bearing estimation in a multipath environment," *IEEE Transactions on Signal Processing*, vol. 36, no. 4, pp. 425–432, 1988.